THE JOURNAL OF PHYSICAL CHEMISTRY A

Article

pubs.acs.org/JPCA

A Comprehensive Analysis in Terms of Molecule-Intrinsic Quasi-Atomic Orbitals. IV. Bond Breaking and Bond Forming along the Dissociative Reaction Path of Dioxetane

Aaron C. West, Michael W. Schmidt, Mark S. Gordon, and Klaus Ruedenberg*

Department of Chemistry and Ames Laboratory USDOE, Iowa State University, Ames, Iowa 50011, United States

ABSTRACT: The quantitative analysis of molecular density matrices in terms of oriented quasi-atomic orbitals (QUAOs) is shown to yield detailed conceptual insight into the dissociation of dioxetane on the basis of ab initio wave functions. The QUAOs persist and can be followed throughout the reaction path. The kinetic bond orders and the orbital populations of the QUAOs quantitatively reveal the changes of the bonding interactions along the reaction path. At the transition state the OO bond is broken, and the molecule becomes a biradical. After the transition state the reaction path bifurcates. The minimum energy path gently descends from the transition state via a valley−ridge inflection point to a second saddle point, from which two new minimum energy paths lead to two equivalent formaldehyde dimers. The CC bond breaks, and the π-bonds of the formaldehyde fragments form in close vicinity of the second saddle point. The changes of the interactions in this region are elucidated by the analysis of the rearrangements of the QUAOs.

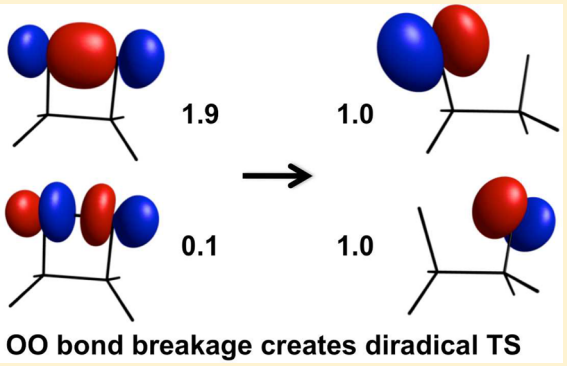

1. INTRODUCTION

The present study is part of a series of investigations aimed at gaining insights into the bonding between atoms in molecules through an analysis of ab initio electron density matrices in terms of rigorous quasi-atomic orbitals (QUAOs). In the first paper,[1] this QUAO analysis was developed for Hartree−Fock wave functions. In the second paper,[2] the QUAO analysis was extended to strongly correlated wave functions. In a third paper,[3] the method was used to elucidate the bonding pattern of the urea molecule.

The object of the present investigation is to exemplify that the analysis in terms of QUAOs can elucidate changes in bonding patterns that occur along reaction paths when bonds break and form. To this end, the minimum-energy path (MEP) for the dissociation of dioxetane $C_2O_2H_4$ into the formaldehyde dimer $(H_2CO)_2$ is examined. A MEP typically consists of a sequence of steepest descent curves that connect critical points, notably minima and saddle points on a potential energy surface (PES).[4] Even though a *dynamic* trajectory would follow a steepest descent curve only if the reaction velocity would be kept infinitesimally small at each point, *MEPs are characteristic structural benchmark features of PESs* that provide an indispensable conceptual basis for understanding and anticipating the set of the actual dynamical trajectories that determine the course of a reaction.

The dissociation of dioxetane is of interest in several contexts. The parent molecule dioxetane as well as its six methylated derivatives were synthesized in 1985 by Adam and Baader,[5] who also showed that the ground states of all of them dissociate between 50 and 70 °C (explosively if not handled carefully) into the respective formaldehyde fragments generating chemiluminescence. Over 99% of the emitted light is due to emission from the lowest triplet (n→π*) state, which represents ∼40% of the formaldehyde product. More complex dioxetane derivatives have also been proposed as being involved in chemiluminescence phenomena.[6,7] The parent molecule is believed to be the simplest known chemiluminescent system.

Dioxetane-like substructures in large bio-organic molecules, which are formed by the attachment of singlet oxygen molecules to certain double bonds, can subsequently fall apart by a dissociation of the dioxetane substructures.[8−11] Such systems are actively studied as carriers for drug delivery.[12] A similar reaction sequence is believed to be responsible for the creation of toxic carbonyls from indocyanine-green, which is widely used in medical diagnosis.[13]

The formaldehyde dimer is held together by weak (C−H···O) hydrogen bonds. This type of bond has attracted considerable attention in the last two decades because it contributes to intermolecular stabilizations in various supramolecular systems.[14−16] For instance, such bonds play a role in crystal packing,[17] in protein conformations,[18] and in the intersheet cohesion that impedes the biomass degradation of cellulose.[19] They have also been implicated in directing organic syntheses.[20] Since the dissociation of dioxetane liberates ∼60 kcal/mol, the dissociative *dynamic* trajectories are expected to

Received: April 8, 2015
Revised: September 14, 2015
Published: September 15, 2015

DOI: 10.1021/acs.jpca.5b03402
J. Phys. Chem. A 2015, 119, 10376−10389

pass the weakly (~4 kcal/mol) bound dimer and go on to the separate monomers.

To understand the mechanism that yields the chemiluminescence from the triplet state of the products, several electronic structure studies of the dissociation of the dioxetane ground state have been performed with successively increasing quantum chemical sophistication, notably by Robb and coworkers[21,22] and by De Vico, Lindh, et al.[23] The dynamics of the dioxetane dissociation have been studied by Farahani, Lindh, et al.[24] on the basis of several hundred trajectories. These recent papers also contain references to prior work. The essential focus of these investigations is (i) the origin of the strong intersystem crossing from the singlet ground-state PES to the lowest triplet PES along the reaction path and (ii) the activation energies for the singlet and triplet dissociations. The MEP of the ground-state dissociation was not followed to the dimer. Accurate calculations of the formaldehyde dimer have recently been made by Dolgonos.[25] The dynamics of a theoretical formation of dioxetane by addition of O_2 to ethylene[26] followed by the dissociation into two formaldehydes has also been investigated.[11,27−30]

The present study is not aimed at exploring the PES features that lead to the chemiluminescence. Rather, the goal is to show that the rigorous quantitative analysis in terms of QUAOs, which has been developed in the preceding papers, is applicable along reaction paths and able to shed light on bond breaking and forming. With this end in mind, the present QUAO analysis focuses on the MEP that stays on the singlet ground-state PES of this reaction, which yields ~60% of the products. Nonetheless, the attributes of this MEP and the methodology used here are also demonstrated to be in accord with the results of the studies mentioned in the preceding paragraph,[21,23,24] which focus on the relation between the singlet and triplet states.

2. ELECTRONIC WAVE FUNCTION

The dissociation of dioxetane into the formaldehyde dimer, which is the focus of the present study, is schematically depicted in Figure 1. In the following, the atoms on the left side of the system will be denoted as O, C, H_1, and H_2, and the atoms on the right side will be denoted as O′, C′, H_1′, and H_2′.

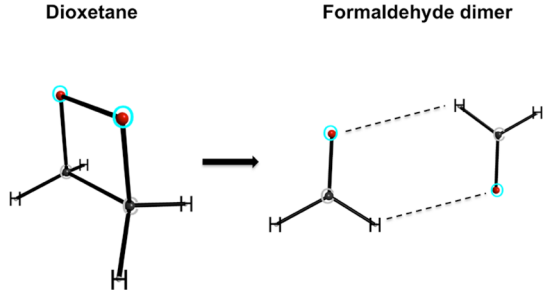

Figure 1. Dissociation of dioxetane into the formaldehyde dimer. All distances, including those between the two formaldehyde molecules, are to scale.

The reactant dioxetane molecule has C_2 symmetry. The C_2 axis goes through the midpoints of the O−O bond and the C−C bond. The O−O bond axis is not parallel to the C−C bond axis, but the OCC′O′ dihedral angle is only 8°.

Since two bonds are broken and two new bonds are formed, the description of the reaction requires a multiconfigurational wave function. To this end, a complete active space wave function with eight electrons in eight orbitals [CAS(8,8)] is used.[31] The valence orbital space is divided into an inactive subspace and an active subspace. For the dioxetane molecule, these two subspaces are chosen as follows:

(i) The inactive valence space consists of eight doubly occupied orbitals, viz.:
- the 2s-type lone pair orbital on each of the two O atoms,
- the 2pπ-type lone pair orbital on each of the two O atoms that is perpendicular to a plane that is approximately spanned by the carbon and oxygen atoms,
- the four bonding orbitals between the two C atoms and the respective four H atoms.

(ii) The active valence space consists of eight orbitals containing 8 electrons, viz., the σ-bonding and antibonding orbitals between C and O, the σ-bonding and antibonding orbitals between C′ and O′, the σ-bonding and antibonding orbitals between C and C′, the σ-bonding and antibonding orbitals between O and O′.

As will become apparent below, the symmetry of the system changes along the reaction path. Nonetheless when, following the reaction path, the reactant orbitals deform, the orbitals can be identified, and the wave function format can be retained. In C_2 symmetry, the specified wave function has 2468 determinants. In C_1 symmetry, it contains 4900 determinants. It will be shown in Section 5 that, in the context of the present study, the 2pπ-type lone pair orbitals on oxygen remain doubly occupied even when they are included in the active space.

In the following discussions, the symbol CAS(m,n) implies a CASSCF(m,n) calculation unless explicitly stated otherwise, where m equals the number of electrons and n equals the number of active orbitals. All quantitative results discussed in the subsequent sections were obtained by calculations with the GAMESS program suite for molecular calculations[32,33] using the Dunning triple-ζ cc-pVTZ basis sets.[34]

3. MINIMUM ENERGY REACTION PATH FOR THE GROUND-STATE DISSOCIATION

The MEP for the dioxetane dissociation on the singlet ground state was calculated in several sections. The changes of the molecular energy along the paths from dioxetane to the dimer product are plotted versus the MEP path length (in angstroms $\times \sqrt{}$amu with amu = atomic mass unit) in Figure 2a,b, where the various sections are distinguished as curves of different colors. To prevent ambiguities in following the orbital deformations, all steepest descent calculations[35] were performed using small step sizes, viz., 0.0265 Å(amu)$^{1/2}$. Approximately 1500 geometries were generated along the entire reaction path.

The Figure 2a shows the entire path. Figure 2b shows an enlargement of the middle part. Eight points are marked by solid dots on these curves: the dioxetane reactant, the transition state (TS), the product dimer, and five additional points (the abbreviation RPP stands for "reaction path point"). It is for these eight points that quantitative values are discussed in the subsequent sections. The energies, the reaction path lengths, and the geometric data of the system at these points are collected in Table 1.

3.1. From the Reactant to the Transition State. The first MEP section goes from dioxetane to the TS. It is the first part of the red curve in Figure 2a. To obtain this section, the geometry of TS was found and optimized. The steepest descent

DOI: 10.1021/acs.jpca.5b03402
J. Phys. Chem. A 2015, 119, 10376−10389

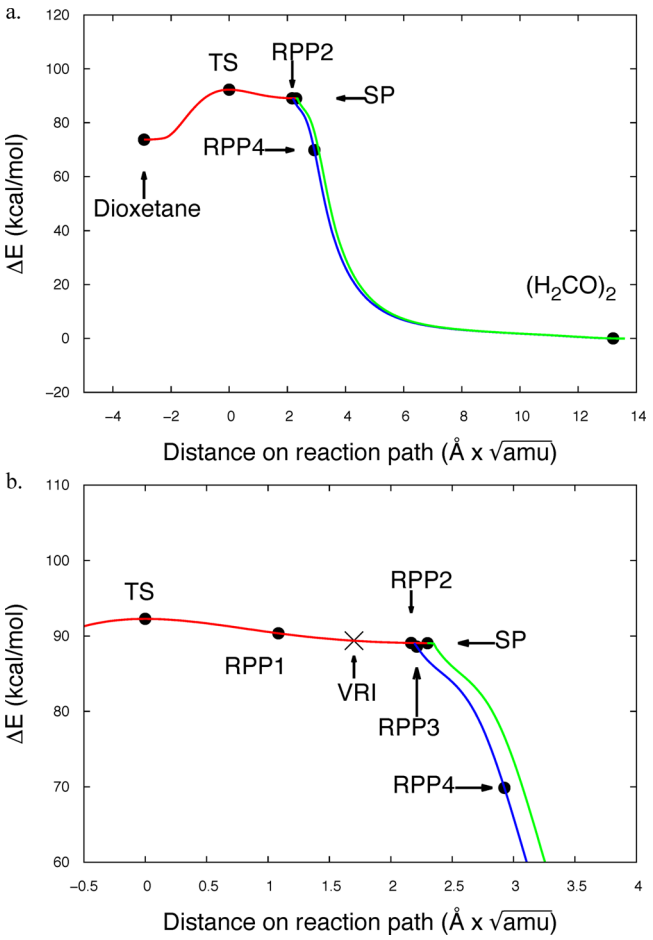

Figure 2. Energy changes along the reaction path of the dissociation of dioxetane to the formaldehyde dimer. The color code is explained in the text. (a) The overall reaction. (b) Enlargement of the section from the transition state (TS) to the fourth reaction path point (RPP4). The points marked by solid dots indicate the geometries for which explicit analyses are presented. The symbol SP indicates the second saddle point. The cross indicates the valley ridge inflection (VRI) point.

from the TS to the dioxetane reactant was determined. The geometry of dioxetane was optimized.

Dioxetane is found to have C_2 symmetry, and the ground state belongs to the ^1A representation. According to Table 1, the CC′ bond length (1.53 Å) is close to that of a typical CC′ single bond (1.54 Å). The OO′ distance (1.52 Å) is markedly larger than the distance in H_2O_2 (1.47 Å). The OO′ bond is thus a weak OO single bond. The CO bond length (1.46 Å) is somewhat longer than the single CO bond length in alcohols (1.43 Å) or ethers (1.42 Å). The lengthening of the OO bond and the CO bond is estimated to relieve the strain of the dioxetane ring by ∼9.41 kcal/mol.[36] Since the OCC′O′ dihedral angle is only ∼8° (third row in Table 1), the four atoms O, C, C′, and O′ form a nearly planar rectangle. Even though the OCC′ angle is close to 90°, the angles OCH_1, OCH_2, and H_1CH_2 are close to tetrahedral.

At TS, the OO′ bond is broken (2.30 Å, fourth row of Table 1 in black bold font). The CC′ bond length has only changed by 0.002 Å. The CO bond has shortened to 1.44 Å, which is close to a typical CO single bond length of 1.43 Å. The angles involving the H atoms have changed very little. The OCC′ angle has opened to 101.6° so that the four bonds emanating from the C atom are moving toward a tetrahedral arrangement. The dihedral angle OCC′O′ (third row in Table 1) has increased considerably to 38°.

The transition state is found to have C_2 symmetry as well. In fact, this molecular symmetry is maintained along the entire MEP that connects the reactant dioxetane with the TS. The wave function continues to have ^1A symmetry.[4,37−41]

3.2. From the Transition State to the Product. *3.2.1. Minimum Energy Path.* The nuclear Hessian at the TS has only one negative eigenvalue, and the corresponding eigenmode belongs to the A representation in the group C_2. The symmetry of the wave functions on the MEPs that leave the TS along this imaginary mode toward product and reactant is therefore also A. Thus, the wave function on the dissociative MEP continues to belong to the ^1A symmetry in the C_2 group.[37] Therefore, the dissociative steepest descent curve was followed under enforcement of C_2 symmetry. The resulting energy changes are displayed by the continuation of the red curve that leads from the TS to the point denoted as SP in Figure 2a,b. This curve has a gentle slope, and the point SP is a minimum in C_2 symmetry.

When the restriction to C_2 symmetry is removed at SP, the nuclear Hessian at this critical point is found to be a saddle point with one negative eigenvalue. The corresponding mode has B symmetry in the C_2 group and is perpendicular to the A mode along which the red MEP arrives at SP. Starting a new steepest descent in C_1 symmetry from SP in the direction of this B symmetry mode generates the MEP that is shown as the green curve in Figure 2a,b. This green MEP leads down a steep slope to the formaldehyde dimer.

In fact, there exist two MEPs that start at SP in opposite directions. They lead to two equivalent dimer minima on the PES. Consequently, there are two groups of *dynamic reaction paths* for the dissociation of dioxetane, which *bifurcate after the transition state TS*. Correspondingly, the red MEP that leads from TS to SP starts in a valley and ends on a ridge. The valley−ridge inflection point,[42−46] where the changeover happens, was determined by finding the point where the projected nuclear Hessian in the space normal to the gradient has a vanishing eigenvalue. This point occurs at 1.70 (Å$\sqrt{}$amu) and is marked by a cross (×) on the red curve. The situation corresponds to Case 2 of the original analysis by Valtazanos and Ruedenberg in ref 42. It is now well-recognized that valley−ridge inflection points play important roles in chemical dynamics.[47−49]

The saddle point SP is of course a transition state for the interconversion between the two equivalent dimers. But it is not a transition state for the dioxetane dissociation. To avoid confusion, the symbol SP is therefore used to denote this saddle point rather than a symbol that contains TS.

It turns out that the described sequential two-part MEP construction, i.e., first along the red MEP in C_2 and then along the green MEP in C_1, is closely simulated by *one* MEP run that starts the steepest descent at the TS immediately in C_1 symmetry, i.e., without enforcement of C_2 symmetry. At first this process follows the red C_2 curve. However, after passing the valley−ridge inflection point, this steepest descent algorithm "falls off the ridge" and finds another, lower steepest descent curve that ends at the dimer minimum. The result of this calculation is displayed as the blue curve on Figure 2a,b. This blue C_1 curve separates from the red C_2 curve at the point RPP2, slightly before the saddle point SP. Its descent to the

DOI: 10.1021/acs.jpca.5b03402
J. Phys. Chem. A 2015, 119, 10376−10389

Table 1. Relative Energies, Interatomic Distances and Angles at Eight Reaction Path Points on the Minimum Energy Path From Dioxetane to the Formaldehyde Dimer

	diox	TS	RPP1	RPP2	SP	RPP3	RPP4	$(H_2CO)_2$
Energy[a]	73.74	92.26	90.35	89.07	89.05	88.59	69.86	0[b]
MEP[c]	−2.932	0	1.085	2.166	2.299	2.211	2.925	13.200
∠OCC′O′ [d]	8.34	37.62	48.26	64.86	67.64	64.96	66.30	180.00
OO′ [e]	1.521	**2.299**	2.653	2.948	2.987	2.950	2.901	3.681
CC′	1.534	1.536	1.540	1.539	1.539	**1.543**	**1.775**	**3.813**
CO	1.464	1.437	1.420	1.418	1.417	**1.416**	**1.295**	**1.218**
C′O′	1.464	1.437	1.420	1.417	1.417	**1.415**	**1.295**	**1.218**
CH_1	1.080	1.082	1.085	1.086	1.086	1.084	1.084	1.085
$C'H'_1$	1.080	1.082	1.085	1.086	1.086	1.085	1.084	1.085
CH_2	1.079	1.081	1.083	1.084	1.084	1.083	1.079	1.088
$C'H'_2$	1.079	1.081	1.083	1.084	1.084	1.083	1.080	1.088
∠OCC′	89.45	101.57	107.87	111.75	112.08	111.71	107.95	68.11
∠O′C′C	89.45	101.57	107.87	111.69	112.08	111.67	107.75	68.11
∠COO′	89.96	72.00	63.83	55.68	35.55	55.68	59.05	74.01
∠C′O′O	89.96	72.00	63.83	55.72	35.55	55.75	59.18	74.01
$\angle OCH_1$	110.82	108.45	106.17	**106.29**	106.02	**107.72**	**116.39**	121.27
$\angle O'C'H'_1$	110.82	108.45	106.17	**105.80**	106.02	**105.86**	**116.32**	121.27
$\angle OCH_2$	111.03	110.56	110.06	**108.32**	108.55	**107.41**	**117.38**	120.90
$\angle O'C'H'_2$	111.03	110.56	110.06	**109.00**	108.55	**109.82**	**117.48**	120.90
$\angle H_1CH_2$	111.31	110.69	109.49	108.58	108.53	108.88	114.80	117.83
$\angle H'_1C'H'_2$	111.31	110.69	109.49	108.63	108.53	108.93	114.81	117.83

[a]Energies relative to $(H_2CO)_2$ in kilocalories per mole. [b]The absolute value of the dimer energy is −227.973 727 8229 hartree. The dimer lies 2.62 kcal/mol below the separated monomers. [c]Distance on the MEP relative to the transition state in angstroms × $(amu)^{1/2}$ where amu = atomic mass unit. [d]Dihedral angle between the CO vector and the C′O′ vector in degrees. [e]All internuclear distances are given in angstroms.

dimer product follows the "accurate" green MEP curve extremely closely.

The physical interactions that are operative in the PES region around the point SP will be elucidated by the QUAO analysis toward the end of Section 4.2. The relation to the work in refs21−23 will be discussed in Section 5.

3.2.2. Geometries. The geometries listed in Table 1 for the various points show that, on the gentle descent from TS to SP, a major geometrical change is the increase of the OCC′O′ dihedral angle. At TS it is 37.6°. At RPP2 it is 64.9°. At SP it is 67.6°. Correspondingly, the OO′ bond length increases by 0.69 Å, the angle OCC′ increases by 11°, and the angle COO′ decreases by 36°.

The CC′ bond remains unbroken from dioxetane to SP. At RPP2 and SP, it has lengthened only by 0.003 Å with respect to the value at TS. Similarly, the CO bonds shorten only by 0.02 Å to become close to the single bond in dimethyl ether (1.42 Å). Even at the beginning of the steep blue and green MEPs that lead from RPP2 and SP, respectively, to the dimer, the CC′ bond remains intact, and the CO bonds remain single bonds: At RPP3 the CC′ bond is still only 0.003 Å longer than a typical single CC′ bond of 1.54 Å, while the CO bond lengths have hardly changed.

It is between RPP3 and RPP4 that the strong covalent CC′ bond breaks, as is evinced by the increase of CC′ from 1.543 to 1.775 Å. Correspondingly, the CO bonds shorten from the single bond length from 1.416 to 1.295 Å, i.e., half way toward the final double bond length of 1.218 Å. These bond length changes are marked in bold type in the upper part of Table 1.

The data listed in Table 1 for the blue MEP of C_1 symmetry that leads from RPP2 to the dimer also exhibit the loss of the higher symmetry. This loss of symmetry is apparent from the differences 0.49°, 1.86°, 0.07° between the two angles $\angle OCH_1$ and $\angle O'C'H'_1$ at the points RPP2, RPP3, and RPP4, respectively, and from the corresponding differences 0.68°, 2.41°, 0.10° between the two angles $\angle OCH_2$ and $\angle O'C'H'_2$ at these points. These differences, which are apparent from the values that are indicated in bold font in the lower part of Table 1, show that the blue C_1 curve has already slightly separated from the red C_2 curve at RPP2 even though the energy difference is less than 6×10^{-5} kcal/mol.

3.3. The Formaldehyde Dimer. As discussed in the preceding section, the reaction path bifurcates, and there are two equivalent product minima. Both of these products are formaldehyde dimers that have C_{2h} symmetry, as is apparent from the values of the angles ∠OCC′, ∠O′C′C, ∠COO′, and ∠C′O′O in Table 1. As shown in Figure 1, all eight atoms of this dimer lie in one plane. The OCC′O′ dihedral angle is 180°. Note that, whereas the dioxetane reactant is a chiral molecule if the nonequivalent hydrogens are tagged as being different, the C_{2h} dimer is not.

The formaldehyde dimer has been the subject of a number of investigations, notably a recent very high-level coupled cluster calculation,[25] which also contains a survey of the previous literature. Considering that the present approach does not include dynamic correlation, the geometric data obtained here for the monomer in the dimer are reasonably close to the coupled cluster values. Table 1 lists CO = 1.218 Å, CH = 1.085 Å, $\angle OCH_1$ = 121.27°, and $\angle OCH_2$ = 120.90°. The corresponding coupled cluster values are 1.210 Å, 1.101 Å, 121.1°, and 121.4°, respectively. (The experimental values for a single formaldehyde molecule[50] are, respectively, 1.206 Å, 1.108 Å, and 116.6°). The distance between the oxygen atom on one monomer and the nearest hydrogen atom on the other monomer is 2.721 Å in the present work and 2.463 Å in the coupled cluster calculation. For the binding energy of the dimer, the present approach yields −2.64 kcal/mol, while the

DOI: 10.1021/acs.jpca.5b03402
J. Phys. Chem. A 2015, 119, 10376−10389

value of −2.32 kcal/mol is obtained for the coupled cluster wave function.

The aforementioned coupled cluster data correspond to the dimer of C_{2h} symmetry. It should be mentioned that the coupled cluster calculation of ref 25 showed (as had previous investigations) that there exists another conformer of the formaldehyde dimer, which has C_s symmetry. In fact, the C_s conformer was found to be 0.3−0.4 kcal/mol lower in energy than the C_{2h} conformer. As yet, the PES that connects the two dimer conformers does not seem to have been explored. They can of course easily interconvert by dissociation and recombination.

4. QUASI-ATOMIC ORBITAL ANALYSIS ALONG THE MINIMUM-ENERGY PATH OF THE GROUND-STATE DISSOCIATION

The present analysis is based on two sets of orbitals:

- The *oriented QUAOs*, which correspond to hybridized free-atom orbitals that are deformed by the chemical environment in the molecule,
- The *split-localized orbitals*, which correspond to bonding, antibonding, and nonbonding (e.g., lone pair and radical) molecular orbitals. The split-localized orbitals can be expressed as superpositions of the QUAOs.

The split-localized orbitals yield a broad picture of the bonding and strong correlation pattern. The QUAOs yield a more detailed analysis. The unique features of the present formulations are the following:

(i) The orbitals are obtained as linear combinations of the MCSCF orbitals that are derived from a calculation in a full molecular valence space, or in an active subspace thereof, which is, for instance, used along a chemical reaction path. For example, the present wave function specified in Section 2 contains only a doubly occupied bonding orbital for each (nonreactive) CH bond so that four orbitals of the full valence space are missing, viz. those that correspond to the antibonding CH orbitals. These lowest unoccupied molecular orbitals are unambiguously identified as *valence virtual orbitals (VVOs)* by the present method,[51] and they are then included in constructing the quasi-atomic and split-localized orbitals.

(ii) The N-electron MCSCF wave function can be expressed in terms of these orbitals.

(iii) The MCSCF energy can be decomposed in terms of contributions from these orbitals. From this energy decomposition, a new energetic characterization of bond strength is derived, the *kinetic bond order*, which is commented on below.

(iv) *No user input (regarding bonding, nonbonding, or other expectations) of any kind whatsoever is part of the internal criteria* that determine the orbitals and their properties.

(v) These criteria are also *basis set independent*, and the orbitals exhibit the same quality for any reasonable working basis.

The objective of the present study is to establish that the application of the devised mathematical formalism (and the automated code) to a not quite trivial case along a reaction path in fact yields data that, on the one hand, fit in with chemical intuition and, on the other hand, provide additional quantitative details.

4.1. Localized Bonding, Antibonding, and Nonbonding Orbitals (Split-Localized Orbitals). The bonding and correlation patterns that are created for dioxetane and for one formaldehyde molecule in the dimer are exhibited by the split-localized valence orbitals that are displayed in Figure 3. Positive

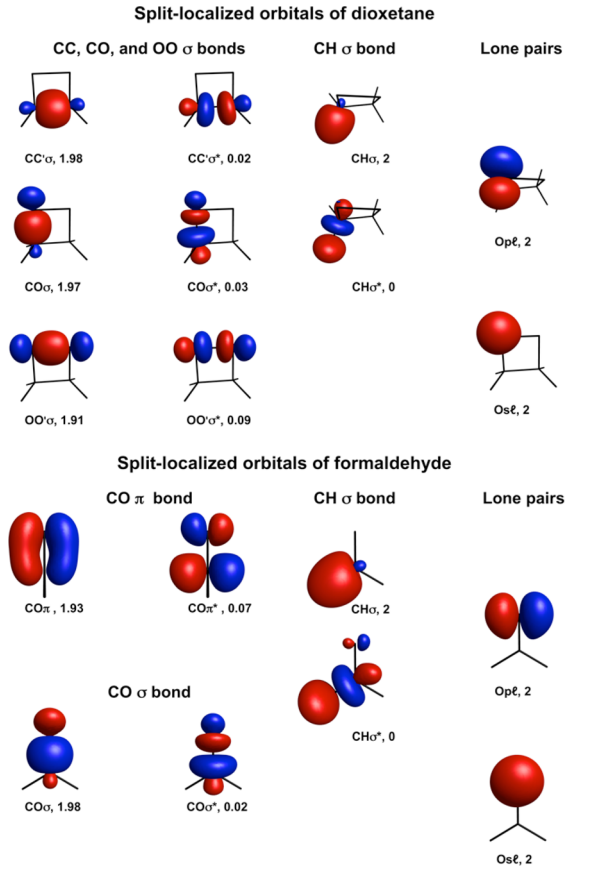

Figure 3. Split-localized orbitals of dioxetane (upper) and of formaldehyde (lower). Orbital labels and occupation numbers are in bold font below each orbital. The contour surfaces correspond to absolute orbital values of 0.1 (electron/bohr^3)$^{1/2}$. Only the orbitals for one of the CH bonds and one of the CO bonds are shown.

lobes are red; negative lobes are blue. The contour surfaces correspond to absolute orbital values of 0.1 bohr$^{-3/2}$. In dioxetane, only symmetry-unique orbitals are shown. Moreover, only one of the two CH bonds on the left carbon is shown. Although the bonds CH_1 and CH_2 differ slightly, the difference is too small to be relevant for the present discussion (see, e.g., the differences involving H_1 and H_2 in Table 1.)

Below the orbital plots, the orbital labels and the orbital occupations (in electron units) are indicated. Each oxygen atom turns out to have a 2s-type lone pair (Os*l*) and a 2p-type lone pair (Op*l*). For each two-center bond, there is a bonding and an antibonding orbital (σ and σ^* for the σ bonds; π and π^* for the π-bonds). Since the CH bonds are described by doubly occupied closed-shell orbitals in the present wave function, the antibonding CHσ^* orbitals are VVOs (see item (i) above in the introductory paragraph before this section), so that their occupations are zero. They are nonetheless relevant for the QUAOs in the next section.

According to the upper panel of Figure 3, each of the eight bonds in dioxetane is established by two electrons, namely, the sum of the occupations of the bonding and the antibonding

DOI: 10.1021/acs.jpca.5b03402
J. Phys. Chem. A 2015, 119, 10376−10389

localized molecular orbitals. The correlating OO′σ* antibonding orbital has a higher occupation (0.09) than the correlating CC′σ* antibonding orbital (0.02) and the correlating COσ* antibonding orbital (0.03). Of the two lone pair orbitals on oxygen, one is s-type, while the other is a 2pπ-type orbital that is essentially perpendicular to the approximate plane spanned by the oxygen and carbon atoms. For the formaldehyde molecule, the lower panel of Figure 3 exhibits the σ-bond and the π-bond between carbon and oxygen as well as the two lone pairs on oxygen. There is more correlation in the π-bond than in the σ-bond, as is the case in many π-bonds (e.g., in ethene and ethyne).

It is apparent that the split-localized orbitals for the lone pairs, for the CO σ-bonds and for the CH bonds in formaldehyde are very similar to those in dioxetane. In fact, these orbitals retain their characters along the entire reaction path. They are therefore not shown for the intermediate geometries. The evolutions of the remaining four split-localized orbitals, which describe the bond breaking and reforming along the dissociation path, are exhibited in Figure 4 for the points denoted as dioxetane, TS, RPP3, RPP4, and $(H_2CO)_2$.

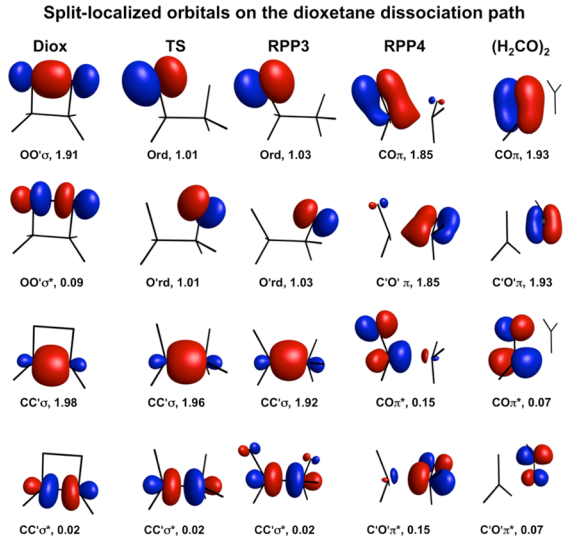

Figure 4. Changes of the four split-localized orbitals that are involved in the bond breaking and forming at five points of the dissociation paths from dioxetane to the formaldehyde dimer. The left CO bond always lies in the plane of the paper. The CC′ bond lies in the plane of the paper except in the last column. The right C′O′ bond lies in the plane of the paper for dioxetane. In going from the column TS, to the column RPP3, to the column RPP4, the atom O′ moves more and more behind the plane of the paper in accordance with the increasing dihedral angle in Table 1. Thus, the CO π (π*) bond in the first (third) row lies in the plane of the paper, whereas the C′O′ π (π*) bond in the second (fourth) row points toward the back. In the last column, the dimer is oriented in such a perspective that both the positive and the negative lobes of the CO π (π*) bonds are shown. The left and right parts of the dimer manifestly have the orientation shown in Figure 1 with an OCC′O′ dihedral angle of 180°.

The orbitals in the dioxetane column of Figure 4 are identical with the corresponding orbitals in Figure 3. At the transition state (TS column of Figure 4), the OO′ bond is broken. Instead of the strongly occupied bonding orbital OO′σ and the weakly occupied antibonding orbital OO′σ* for this bond in the dioxetane column, the TS column shows a singly occupied orbital Ord on the left oxygen and a singly occupied orbital O′rd on the right oxygen. *At the transition state the molecule is thus a biradical*, which is implied by letters "rd" in the orbital labels. *This transition from a bonding/antibonding orbital pair to two radical orbitals is automatically produced by the present analysis.*[52] The same split-orbital structure persists along the reaction path to the RPP3 column of Figure 4.

In the next-to-last paragraph of Section 3.2 above, the increase in the CC′ bond length from 1.543 to 1.775 Å was taken as implying that the breakage of this bond occurs between RPP3 and RPP4. This inference is confirmed by the fact that the split-localized orbitals at RPP4 differ qualitatively from those at RPP3. At RPP4, the CC′ bonding and antibonding orbitals and the oxygen radical orbitals have disappeared. Instead, a π-bonding orbital and a π-antibonding orbital have formed on each of the formaldehyde-like fragments. The QUAO analysis below provides more detail on this change. This split-localized structure is retained from RPP4 onward, as the two fragments separate and rotate to have antiparallel CO bonds.

4.2. Oriented Quasi-Atomic Orbitals. Figure 5 displays the oriented QUAOs of dioxetane and of formaldehyde.[53] In dioxetane, only the symmetry-unique orbitals and one CH bond are shown, as explained at the beginning of the preceding Section 4.1, where the format and the specifications of the plots

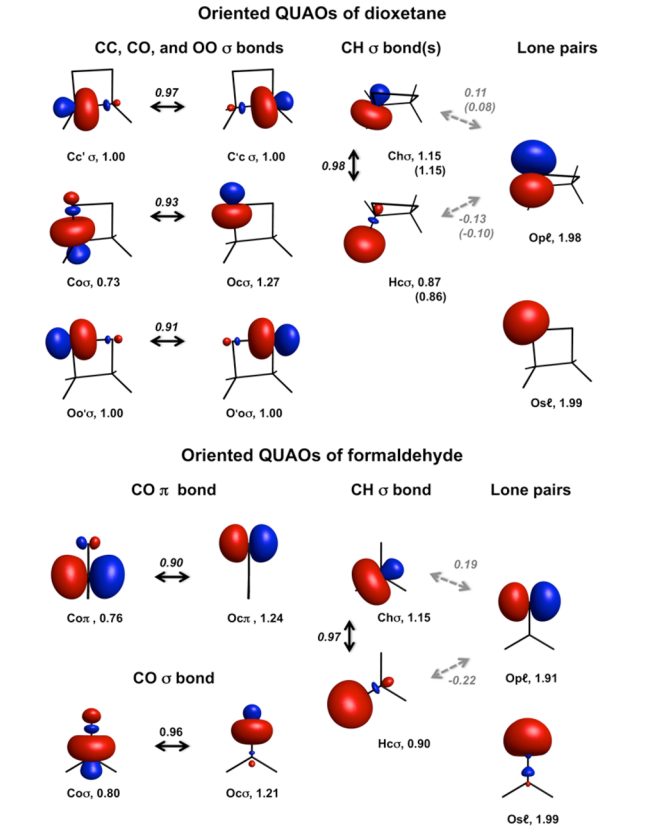

Figure 5. Oriented QUAOs of the reactant dioxetane at its minimum energy geometry (upper) and the formaldehyde molecule (lower). Occupations are in bold font below each orbital next to the orbital symbol. Strong (weak) bonding is indicated by a solid black (dashed gray) arrow. The bond orders are indicated next to the respective arrows. For Chσ and Hcσ in dioxetane, the values without and with parentheses correspond to the CH_1 bond and the CH_2 bond, respectively. Only the QUAOs for one of the CH bonds and for one of the CO bonds are shown.

DOI: 10.1021/acs.jpca.5b03402
J. Phys. Chem. A 2015, 119, 10376−10389

are also discussed. As in Figures 3 and 4, the orbital labels and the orbital occupations are listed below the orbital plots. The QUAOs that are bonded are connected by arrows. The respective bond orders are shown next to these arrows.

The symbols that label the QUAOs in the figure imply their chemical functions according to the following scheme. Each symbol consists of several parts. The first part is always the atomic symbol of the atom *on which QUAO is located*. If the QUAO is a bonding orbital, then the second part of the QUAO symbol is the atomic symbol, *written in lower case font*, of the atom *to which this QUAO establishes a bond*. The third part of the QUAO symbol contains a characterization of the bond type. For instance, Coπ denotes a QUAO on a carbon atom that establishes a π-bond to an oxygen atom. Mgbrσ would denote a QUAO on magnesium establishing a σ-bond to bromine. If a nonbonded QUAO contains close to two electrons, then the second part of the QUAO symbol characterizes it as a lone pair. Thus, Os*l*, Op*l* denote an s-type, p-type lone pair on oxygen. If a nonbonded QUAO contains approximately one electron, then the second part of the QUAO symbol characterizes it as a radical. For instance, Oprd would denote a p-type radical QUAO on an oxygen atom.

It is apparent from Figure 5 that the corresponding oriented QUAOs in dioxetane and in formaldehyde are very similar. In fact, it is found that all QUAOs maintain their essential characteristics along the entire reaction path, although their directions change as the dihedral angle OCC′O′ opens. Therefore, only the evolution of the QUAOs whose bonding interactions change dramatically will be examined in detail.

In Section 3.2.2 and in the last two paragraphs of Section 4.1, it was found that the OO′ bond of dioxetane breaks first, which results in a biradical. Somewhat later, the CC′ bond breaks as well, and the π-bonds form in the two formaldehydes. An intuitive anticipation regarding the evolution of the QUAOs on the left side of the molecule, say, would be as follows. After the OO′ bond is broken, the QUAO Oo′σ, which had been bonded to the O′ atom in dioxetane, becomes a radical orbital on O, and its label should therefore be changed to Ord. After the CC′ bond is broken as well, this oxygen QUAO forms a π-bond with the carbon QUAO Cc′σ, which had been bonded to the C′ atom in dioxetane. Thus, the labels Ord and Cc′σ should then be changed to Ocπ and Coπ, respectively. (Analogous arguments apply of course to the right side of the molecule.) These labeling changes are used in Figure 6, in which each row exhibits the evolution of one of the four oriented QUAOs whose bonding interactions change along the reaction path. Moreover, on the left side of the figure at the beginning of each row of labels, the duplicate labels Ov, O′v, Cw, and C′w were added as convenient collective descriptors, as follows:

$$\mathrm{Ov} \equiv [\mathrm{Oo'}\sigma \text{ in dioxetane; Ord from TS to RPP3; Oc}\pi \text{ from RPP4 to } (\mathrm{H_2CO})_2]$$

$$\mathrm{O'v} \equiv [\mathrm{O'o}\sigma \text{ in dioxetane; O' rd from TS to RPP3; O'c'}\pi \text{ from RPP4 to } (\mathrm{H_2CO})_2]$$

$$\mathrm{Cw} \equiv [\mathrm{Cc'}\sigma \text{ from dioxetane to RPP3; Co}\pi \text{ from RPP4 to } (\mathrm{H_2CO})_2]$$

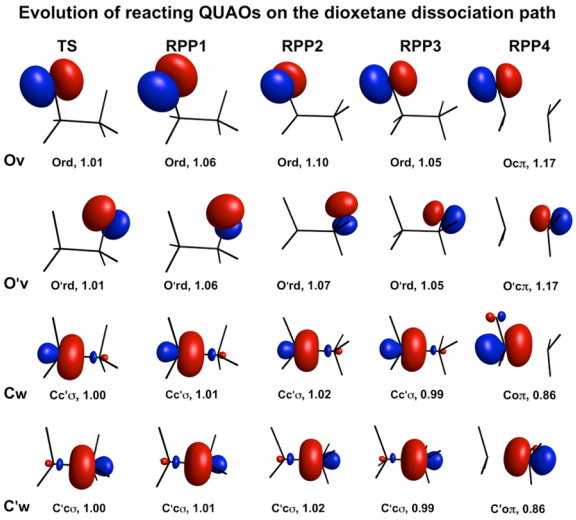

Figure 6. (upper two rows) The evolution of the oriented QUAOs Ov and O′v of the molecule for five points on the dissociation paths from dioxetane to the formaldehyde dimer. (lower two rows) The evolution of the Cw and C′w orbitals. The positions of the atoms with respect to the plane of the paper are the same as described in Figure 4. Accordingly, the O′v radical orbital in the second row moves to the back of the paper in going from TS to RPP4.

$$\mathrm{C'w} \equiv [\mathrm{C'c}\sigma \text{ from dioxetane to RPP3; C'o'}\pi \text{ from RPP4 to } (\mathrm{H_2CO})_2]$$

The QUAOs Cw and C′w on the carbon atoms are seen to change very little along the reaction path from TS to RPP4. In contrast, the changes in the QUAOs Ov and O′v on the oxygen atoms are small only from TS to RPP2.

However, from RPP2 to RPP3, the orientation of Ord in Figure 6 appears to switch by 90° even though the points RPP2 and RPP3 lie extremely close to each other, as is apparent from Figure 2 and Table 1. (The same holds of course for O′rd.) A closer examination of this range shows that the intuitive interpretation that was put forth in the preceding paragraph must be by considering also the doubly occupied lone pair QUAO on oxygen, which is denoted as Op*l* on Figure 5. To elucidate the situation, Figure 7 shows the three orbitals Op*l*, Ord, and Ocπ

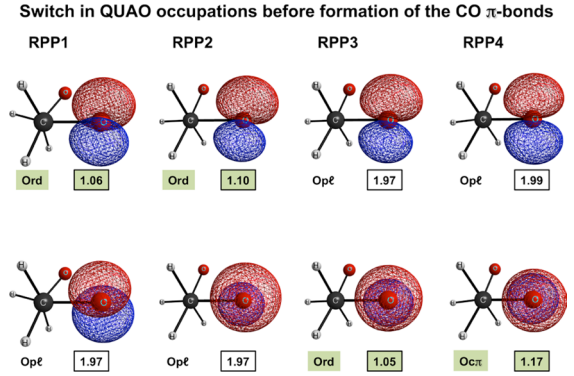

Figure 7. P-type oriented QUAOs on oxygen at the reaction path points (RPPs) RPP1 to RPP4. The line of sight is parallel to the CC bond so that the two carbon atoms lie on top of each other. The red lobes point toward the viewer; the blue lobes point toward the back. The occupations are encased in boxes to emphasize the occupation switch before the formation of the CO π-bonds at RPP4.

DOI: 10.1021/acs.jpca.5b03402
J. Phys. Chem. A 2015, 119, 10376−10389

Table 2. Bond Orders for Oriented Quasi-Atomic Orbital Pairs at Several Reaction Path Points on the Dioxetane Dissociation Path

QUAO pairs		diox	TS	RPP1	RPP2	RPP3	RPP4	$(H_2CO)_2$
				|Bond Order| > 0.30[a,b]				
Ov[c]	O′v	**0.907**	0.302	[0.079]	[−0.043]	[−0.133]	[−0.341]	
Cw[d]	Ov		0.077	0.065	[0.023]	0.211	**0.686**	**0.902**
Cw	C′w	**0.974**	**0.963**	**0.960**	**0.961**	**0.934**	**0.554**	
Coσ	Ocσ	**0.927**	**0.931**	**0.935**	**0.935**	**0.935**	**0.951**	**0.958**
H_1cσ	$Ch_1\sigma$	**0.976**	**0.974**	**0.970**	**0.970**	**0.972**	**0.960**	**0.965**
H_2cσ	$Ch_2\sigma$	**0.978**	**0.974**	**0.973**	**0.970**	**0.970**	**0.963**	**0.967**
				0.02 < |Bond Order| < 0.30[e,b]				
$Ch_1\sigma$	Ord		−0.117	−0.150	−0.148	[−0.058]		
$Ch_2\sigma$	Ord			[0.056]	0.090	−0.086		
H_1cσ	Opl	0.127	[−0.052]			−0.139	−0.185	0.207
H′$_1$c′σ	O′pl	−0.127	[0.052]			[0.091]	0.184	−0.207
H′$_2$c′σ	O′pl	[0.099]	−0.144	−0.133	[0.098]	−0.141	−0.177	0.217
H_2cσ	Opl	[−0.099]	0.144	0.133	[0.078]	[0.097]	0.177	−0.217
Cc′σ	Opl		[0.046]	0.092	0.129			
$Ch_1\sigma$	Opl	−0.107	[0.048]		[−0.031]	0.116	0.159	−0.180
$Ch_2\sigma$	Opl	0.082	−0.124	−0.119	−0.071	−0.085	0.153	0.193
C′h′$_2\sigma$	Coπ						0.095	
C′o′σ	Coσ	0.054	[0.055]	[0.041]	[0.021]	[0.021]		
C′h′$_1\sigma$	Coσ		−0.085	−0.095	−0.103	−0.105	[−0.065]	
C′h′$_2\sigma$	$Ch_2\sigma$	[−0.062]	−0.100	−0.102	−0.105	−0.106	[0.056]	
Ord[f]	Osl		[−0.083]	0.197	0.270	[−0.148]		
O′rd	O′sl		[−0.083]	0.197	−0.221	[−0.154]		

[a]Meaning: in this section, an entire row is shown if any bond order in it has an absolute value ≥0.3. [b]Enclosure in brackets implies that |KBO| = |0.1 × kinetic energy integral × bond order| ≤ 0.63 kcal/mol. [c]The orbital Ov indicates changes from Oo′σ (for dioxetane) to Ord (for TS) to Ocπ (for RPP4 and $(H_2CO)_2$). The orbital symbol Ord is defined in footnote f. [d]The orbital Cw changes from Cc′σ (for dioxetane, TS, and RPP3) to Coπ (for RPP4 and $(H_2CO)_2$). [e]This section contains all cases with 0.02 < |bond order| < 0.30, unless they occur already in the upper section. [f]The orbital symbol Ord denotes the nonbonded, singly occupied radical orbital on oxygen.

at the points RPP1, RPP2, RPP3, and RPP4. In this figure the line of sight is parallel to the CC′ bond so that the two carbon atoms lie on top of each other; the oxygen O atom (with the orbital) and the hydrogen atoms H_1 and H_2 lie somewhat in front of the plane of the paper. *Note that the QUAOs are arranged as follows in this Figure*:

At RPP1 and RPP2 the upper row displays the radical orbital Ord, and the lower row displays the lone-pair orbital Opl.

In contrast, at RPP3 the upper row displays the lone-pair orbital Opl, while the lower row displays the radical orbital Ord.

At RPP4 the upper row displays the lone-pair orbital Opl, and the lower row displays the π-bonding orbital Ocπ.

Each QUAO is identified by its symbol below the plot. The boxes contain the occupations, which confirm the radical (rd), lone pair (l) and bonding (Ocπ) character of the respective orbitals.

In each row of Figure 7, the shapes of the orbitals are seen to vary very little. But the occupancies switch between RPP2 and RPP3. The upper orbital switches from single to double occupancy, and the lower orbital switches from double to single occupancy. This switch suggests the following changes in the interactions in this region of the reaction path. Since the orbitals in the lower row are pointing in a direction nearly perpendicular to the plane of the paper, they clearly have the orientation that is appropriate for π-bonding to the adjacent carbon atom when the orbital is singly occupied. But from TS to RPP2, the CC′ σ-pair bond remains strong and does not allow the Cc′σ QUAO on carbon to get involved into any π-bonding with the oxygen atom. In this situation, the oxygen orbital in the upper row of Figure 7 remains a singly occupied Ord QUAO because its orientation is suited for longer-range (weak) interactions with other parts of the molecule. Between RPP2 and RPP3, however, the CC′ σ-bond becomes somewhat longer and weaker, so that the Cc′σ QUAO on carbon has now some freedom to engage in a bonding interaction with the oxygen QUAO of the lower row of Figure 7. To this end, this QUAO then becomes singly occupied, and the orbital in the upper row is forced to become the doubly occupied Opl QUAO. The bond order analysis in the next section confirms this interpretation.

While the point RPP2 still practically lies on the red C_2 MEP (see Figure 2), a larger step down the blue C_1 MEP has been taken at the point RPP3. From this observation, the following inferences can be drawn. Along the gently sloping red C_2 descent from TS to the saddle point SP, various weak long-range interactions of the singly occupied radical orbital in the upper row of Figure 7 prevail as long as the CC bond stays sufficiently short and the OCC′O′ dihedral angle is sufficiently small. But on the steep descent from SP or RPP2 along the green or blue C_1 curves to the dimer, when the CC bond elongates and the dihedral angle increases, the covalent CO π-bonding interactions of the singly occupied QUAO in the lower row of Figure 7 dominate. The fact that the dissociative MEP consists of two sequential MEPs with different characteristics is thus related to the fact that the interactions of two different singly occupied oxygen QUAO sets are involved in the bonding interactions on these two MEP sections.

4.3. Bond Order Analysis. In ab initio wave functions, the essential contributions to covalent bonding come from the

DOI: 10.1021/acs.jpca.5b03402
J. Phys. Chem. A 2015, 119, 10376−10389

Table 3. Kinetic Bond Orders (KBOs) = 0.1 × Kinetic Integrals × Bond Orders (in kcal/mol) for Oriented Quasi-Atomic Orbital Pairs at Several Reaction Path Points on the Dissociation Path

orbital pairs		diox	TS	RPP1	RPP2	RPP3	RPP4	$(H_2CO)_2$
				|Bond Order| > 0.30[a,b]				
Ov[c]	O′v	**−55.66**	−4.83	[−0.44]	[−0.13]	[0.13]	[0.50]	
Cw[d]	Ov		−1.07	−0.69	[−0.13]	−4.89	**−29.30**	**−47.06**
Cw	C′w	**−59.99**	**−60.49**	**−62.31**	**−63.88**	**−54.09**	**−18.64**	
Coσ	Ocσ	**−76.74**	**−78.06**	**−80.82**	**−81.95**	**−79.38**	**−84.90**	**−93.75**
$H_1c\sigma$	$Ch_1\sigma$	**−36.40**	**−36.27**	**−35.77**	**−35.58**	**−35.64**	**−35.02**	**−36.52**
$H_2c\sigma$	$Ch_2\sigma$	**−36.77**	**−35.89**	**−35.83**	**−35.58**	**−35.27**	**-35.14**	**−36.46**
				0.02 < |Bond Order| < 0.30[e,b]				
$Ch_1\sigma$	Ord		−1.57	−2.45	−2.38	[−0.38]		
$Ch_2\sigma$	Ord			[−0.44]	−1.07	−0.82		
$H_1c\sigma$	Op*l*	−0.75	[−0.13]			−0.88	−1.82	−2.51
$H'_1c'\sigma$	O′p*l*	−0.75	[−0.13]			[−0.38]	−1.82	−2.51
$H'_2c'\sigma$	O′p*l*	[−0.50]	−1.00	−0.88	[−0.44]	−1.00	−1.69	−2.64
$H_2c\sigma$	Op*l*	[−0.50]	−1.00	−0.88	[−0.25]	[−0.44]	−1.69	−2.64
Cc′σ	Op*l*		[−0.31]	−0.94	−1.44			
$Ch_1\sigma$	Op*l*	−1.57	[−0.44]		[−0.13]	−1.82	−3.07	−3.89
$Ch_2\sigma$	Op*l*	−1.07	−1.95	−1.82	−0.75	−1.13	−2.89	−4.27
C′$h'_2\sigma$	Coπ						−0.94	
C′o′σ	Coσ	−0.69	[−0.63]	[−0.38]	[−0.13]	[−0.13]		
C′$h'_1\sigma$	Coσ		−0.69	−0.88	−1.07	−1.07	[−0.38]	
C′$h'_2\sigma$	$Ch_2\sigma$	[−0.31]	−0.88	−0.94	−1.00	−1.00	[−0.19]	
Ord[f]	Os*l*		[0.25]	0.94	1.44	[0.38]		
O′rd	O′s*l*		[0.25]	0.94	1.07	[0.38]		

[a]Meaning: in this section, an entire row is shown if any bond order in it has an absolute value ≥0.3. [b]The KBO is enclosed in brackets if |KBO| ≤ 0.63 kcal/mol. [c]The orbital Ov changes from Oo′σ (for dioxetane) to Ocπ (for RPP4 and $(H_2CO)_2$). The orbital symbol Ord is defined in footnote f. [d]The orbital Cw changes from Cc′σ (for dioxetane, TS, and RPP3) to Coπ (for RPP4 and $(H_2CO)_2$). [e]This section contains all cases with 0.02 < |bond order| < 0.30, unless they occur already in the upper section. [f]The orbital symbol Ord denotes the nonbonded, singly occupied radical orbital on oxygen.

kinetic interference energies between atomic orbitals.[54,55] For the orthogonal QUAOs, these energies are simply the products of the interatomic elements of the density matrix, commonly denoted as bond orders, and the kinetic energy integrals between the corresponding orbitals. The assessment of bonding by means of the "density bond orders" goes back to Coulson and co-workers.[56,57] In the second paper of this series, we introduced[58] the *kinetic bond orders* (KBOs), which are scaled kinetic interference energies, as energetic indicators of the bonding strength between QUAOs. The KBO signs are independent of the phases of the QUAOs.

The evolution of the bond orders between the oriented QUAOs along the reaction paths is exhibited in Tables 2 and 3. Table 2 lists the bond orders $p_{Aa,Bb}$. Table 3 lists the KBOs $k_{Aa,Bb}$. The upper parts of these tables list the bond orders that account for the strong bonds and their changes. The lower parts of the tables document that the remaining bond orders are small.

Each row in these tables corresponds to one *pair* of oriented QUAOs, which are specified by their labels at the beginning of each row. The QUAO labels are the same as those used in Figures 5 and 6. The collective duplicate QUAO labels Ov, O′v, Cw, and C′w are those introduced in Figure 6 and explained at the end of the fourth paragraph of the preceding Section 4.2. In both tables, the upper part contains the rows for all QUAO pairs that have a bond order $p_{Aa,Bb}$ larger than 0.3 in absolute magnitude *for at least one point on the* reaction *path, that is, in at least one column of that row*. In both tables, the lower part contains all cases where the bond order $p_{Aa,Bb}$ lies between 0.02 and 0.3 in absolute magnitude for any orbital pair that is not listed in the upper part. In both tables, the values are enclosed in brackets when the corresponding KBO value is less than 0.63 kcal/mol in magnitude. No entry is made when the KBO value is less than 0.63 kcal/mol in magnitude.

In both Tables 2 and 3, the strong bond orders, which are indicated by bold font, clearly determine the bonding pattern of the system at all stages along the dissociation path. A comparison of the two tables furthermore shows that the KBOs make sharper distinctions than do the density bond orders between different bonds in the same system and between analogous bonds at different stages of the dissociation. *Note that all but two of the interatomic KBO values are negative, i.e., bonding*, the two exceptions (Ov−O′v at RPP3 and RPP4) being less than 0.63 kcal/mol. Only the *intra-atomic* KBO interactions Ord−Os*l* in the last two rows of Table 3 have positive values larger than 0.6 kcal/mol. In the following, therefore, only the KBOs are discussed.

Table 3 shows that the CH bonds retain their strength throughout the dissociation. The CO σ-bonds increase their strength from −76.74 kcal/mol in dioxetane to −93.75 kcal/mol in the formaldehyde dimer, in agreement with the bond shortening from 1.464 to1.218 Å listed in Table 1.

In dioxetane, the QUAO Ov is Oo′σ and binds to the corresponding QUAO on the other oxygen, O′v = O′oσ, with a KBO of −55.66 kcal/mol. At the transition state TS, the QUAO Ov has become the radical QUAO Ord, which has only a KBO of −4.83 kcal/mol with the corresponding radical QUAO O′v = O′rd on the other oxygen. For RPP1 and beyond, the KBO between Ov and O′v drops below 0.63 kcal/mol in absolute value. From TS to RPP2 there are however

DOI: 10.1021/acs.jpca.5b03402
J. Phys. Chem. A 2015, 119, 10376−10389

Table 4. Valence Populations of Oriented Quasi-Atomic Orbitals along the Dissociation Path of Dioxetane

	diox	TS	RPP1	RPP2	RPP3	RPP4	$(H_2CO)_2$
Ocσ	1.269	1.262	1.259	1.260	1.253	1.210	1.208
Coσ	0.731	0.743	0.749	0.750	0.758	0.798	0.796
COσ[a]	2.000	2.005	2.008	2.010	2.011	2.008	2.004
Cw[b]	1.002	1.001	1.011	1.017	0.990	0.861	0.762
Ov[c]	1.002	1.014	1.058	1.097	1.045	1.170	1.238
$Ch_1\sigma$	1.147	1.139	1.132	1.130	1.138	1.142	1.171
$H_1c\sigma$	0.867	0.863	0.857	0.861	0.869	0.867	0.875
$Ch_2\sigma$	1.148	1.143	1.140	1.140	1.144	1.160	1.151
$H_2c\sigma$	0.864	0.875	0.874	0.863	0.862	0.861	0.895
$\langle CH\rangle$[d]	2.013	2.010	2.002	1.997	2.007	2.015	2.046
$\langle \Delta CH\rangle$[e]	0.141	0.136	0.135	0.137	0.138	0.144	0.138
Op*l*	1.977	1.973	1.967	1.971	1.973	1.941	1.915
Os*l*	1.992	1.986	1.952	1.910	1.970	1.991	1.990
O	6.241	6.236	6.237	6.239	6.241	6.311	6.350
C	4.028	4.026	4.032	4.036	4.030	3.961	3.880
H_1	0.867	0.863	0.857	0.861	0.869	0.867	0.875
H_2	0.864	0.875	0.874	0.863	0.862	0.861	0.895

[a]Total CO σ-bond population = sum of preceding two rows. [b]Cw = Cc′σ from diox to RPP3. Cw = Coπ for RPP4, $(H_2CO)_2$. [c]Ov = Oo′σ for diox. Ov = Ord from TS to RPP3. Ov = Ocπ for RPP4, $(H_2CO)_2$. [d]Average population of CH bond = (sum of preceding four rows)/2. [e]Average H → C charge transfer per CH bond = $(Ch_1\sigma - H_1c\sigma + Ch_2\sigma - H_2c\sigma)/4$.

some vicinal interactions between Ov = Ord and $Ch_1\sigma$ (−1.57, −2.45, −2.38 kcal/mol in row 7 of Table 3), which contribute to the persistence of the Ord orbital as was discussed in the last two paragraphs of Section 4.2.

The QUAO Cw is Cc′σ in dioxetane and binds to the corresponding QUAO C′w = C′cσ on the other carbon with a KBO of −59.99 kcal/mol. This interaction persists through the points TS, RPP1, and RPP2. At RPP3, this KBO is somewhat weaker (−54.09 kcal/mol), and there is an incipient interaction (−4.89 kcal/mol) between the QUAO Cw = Cc′σ and the QUAO Ov = Ord. As discussed in the last two paragraphs of Section 4.2, the orbital Ord has actually switched shape with the orbital Op*l* at this point.

At RPP4, the CC′ bonding interaction between Cw and C′w is significantly weaker (−18.64 kcal/mol) than the interaction of Cw with the Ov orbital (−29.30 kcal/mol). Thus, the orbital Cw has become mainly Coπ, and the orbital Ov has become Ocπ; that is, the CO π-bonds have begun to form. For the formaldehyde dimer, the KBO for the CO π-bond is −47.06 kcal/mol, and the KBO between Cw and C′w has dwindled to less than 0.06 kcal/mol. This changeover agrees with the previous conclusion that the CC′ bond breaks and the CO π-bonds begin to form between RPP3 and RPP4.

As in other organic molecules, the lone-pair QUAOs on oxygen are involved in vicinal interactions. Here, they occur with the CH bonds. They are listed in rows 9 to 15 of Table 3. These vicinal KBOs are largest in the formaldehyde dimer, but they still are much smaller (−2.51 to −4.27 kcal/mol) than the corresponding vicinal KBOs in urea (−17.88 kcal/mol), which involve the CN bonds.[3]

In the formaldehyde dimer, the bond orders between the oxygen lone pair QUAOs on one monomer and the QUAO of the nearest hydrogen on the other monomer are 0.03 and 0.04. The corresponding KBOs are found to be 0.25 and 0.13 kcal/mol. These values are more than an order of magnitude smaller than those for weak vicinal bonding interactions. No covalent binding through electron sharing exists therefore between these atoms. The source of the cohesion between the two monomers was identified by a calculation using the Effective Fragment Potential method.[59,60] On the basis of the present dimer geometry, this approach yielded an attractive dimer interaction energy of 5.21 kcal/mol, of which over 80% is of electrostatic origin. This conclusion is in agreement with previous studies of other (C−H···O) hydrogen bonds.[61]

4.4. Population Analysis. The evolution of the orbital occupations of the oriented QUAOs along the reaction path is documented in Table 4. Only the approximately symmetry unique orbitals are listed. The charge transfer values that are inferred from this table in the following discussion are based on assuming the following reference populations in dioxetane: The occupancy 2 for the four oxygen lone pair QUAOs Op*l*, Os*l*, O′p*l*, O′s*l*, and the occupancy 1 for all remaining oriented QUAOs, namely the σ-bonding QUAOs.

The first three rows of Table 4 pertain to the COσ bond. The total population in this bond (3rd row) remains very slightly above two electrons along the entire reaction path. But the transfer of charge from the Coσ orbital to the Ocσ orbital, which is 0.269e for dioxetane, decreases from RPP3 to RPP4 to $(H_2CO)_2$, where it is 0.208e. This decrease in the C to O σ-charge transfer is presumably related to the increase in charge transfer to the oxygen atom through the π-bond, which starts to form between RPP3 and RPP4, as noted in the subsequent paragraphs.

The orbital Cw in the fourth row maintains the CC′σ bond from dioxetane to RPP3. In this range Cw is the oriented QUAO Cc′σ, and its occupation stays very close to 1. From RPP3 to RPP4 to $(H_2CO)_2$, the CO π-bond forms, Cw becomes the Coπ orbital, and charge is transferred through the π-bond onto the oxygen. As a result, the occupation of Cw has decreased to 0.762e in $(H_2CO)_2$.

The orbital Ov in the fifth row is the oriented QUAO Oo′σ in dioxetane, where it establishes the OO′ σ-bond with an occupation of essentially one electron. At the transition state TS, Ov has become Ord, the oriented radical QUAO. From TS to RPP3, the QUAO Ov retains this character, and its occupation increases somewhat. From RPP3 to RPP4 to $(H_2CO)_2$, the CO π-bond forms so that Ov becomes Ocπ, and

DOI: 10.1021/acs.jpca.5b03402
J. Phys. Chem. A 2015, 119, 10376−10389

Table 5. Comparison of Values (in kcal/mol) Obtained by Different Methods for Relevant Energy Differences on the Minimum Energy Path of the Ground State Dissociation of Dioxetane

level of correlation	basis set	dissociation energy[a]	dissociation barrier[b]	biradical descent[c]
CASSCF(8,8)[d]	cc-pVTZ[e]	71.16	18.51	−3.20
CASCI(12,10)[d]	cc-pVTZ[e]	70.78	18.76	−3.83
CAS(12,10)+MP2[f]	6-31+G*[f]	61.43[g]	17.63[h]	−9.29[i]
MS-CASPT2[j]	ANO-TZ[k]	50.08[l]	23.47	−5.65[m]
experiment		63.00[n]	22.72[o]	

[a]Dissociation energy = E(dioxetane) − 2 × E(formaldehyde). [b]Dissociation barrier = E(transition state TS) − E(dioxetane). [c]Drop in energy on the gentle descent in the biradical part of the MEP = E(TS) − E(SP). [d]The present work using GAMESS. See text. [e]Dunning correlation consistent cc-pVTZ basis (ref 34). [f]Work of refs 21 and 22 using GAUSSIAN 94. [g]From ref 21. [h]From ref 22. [i]Calculated from numerical data given in Figure 2a of ref 22. [j]Work of ref 23 using MOLCAS. [k]This abbreviation implies the ANO-RCC basis with [4s3p2d1f] contraction for C and O, and [3s2p1d] contraction for H. [l]From Supporting Information of ref 23. [m]Estimated from Figures 4, 5, and 6a,b in ref 23. [n]From citation in ref 21. [o]From ref 5.

its occupation increases strongly to 1.238e due to charge transfer from the carbon atom.

Rows 6 to 9 of Table 4 show the occupations of the oriented QUAOs that form the two CH bonds that involve one carbon on the left side of the molecule. Row 10 lists the average of the total populations of these two CH bonds, that is, $(Ch_1\sigma + H_1c\sigma + Ch_2\sigma + H_2c\sigma)/2$. It is slightly larger than 2 for most of the reaction path. It is distinctly larger in $(H_2CO)_2$ than in dioxetane. There is a considerable charge transfer from the hydrogens to the carbon atoms along the entire reaction path. As a measure of the average charge transfer per CH bond, the quantity $\langle \Delta CH \rangle = (Ch_1\sigma - H_1c\sigma + Ch_2\sigma - H_2c\sigma)/4$ is listed in row 11. It is seen to be ∼0.14e.

The charge excess beyond 2 in the CH bonds is mainly provided by a decrease in the occupations of the Op*l* lone pair orbital and, to some degree, of the Os*l* lone pair orbital. This inference follows from the occupations of Op*l* and Os*l*, which are listed in the 12th and 13th rows of the table. Charge transfers of this type mediate vicinal interactions, as has been discussed in some detail for the urea molecule.[3] For Op*l*, the occupation deficit from 2 increases considerably from dioxetane (0.023) to the formaldehyde dimer (0.085), corresponding to the increase in the vicinal interactions noted in the next-to-last paragraph of Section 4.3.

The last four rows of Table 4 list the total atomic valence populations of O, C, and the two hydrogen atoms that are bonded to this carbon. From dioxetane to RPP3 these values vary relatively little. From RPP3 to RPP4 to $(H_2CO)_2$, the oxygen population increases by ∼0.11e, the carbon population decreases by 0.15e, and the total population of both hydrogens increases by 0.04e.

5. RELATION TO PREVIOUS WORK

All previous work on the dissociation of dioxetane has focused on explaining the chemiluminescence. This phenomenon is not the object of the present inquiry. The following comments are limited to showing that the MEP analyzed in the preceding sections and the method of its calculation are consistent with the results in the recent previous work.[21,23] Three comparisons are made.

(i) In the cited investigations,[21,23] the p-type lone pairs on the oxygen atoms were included in the active space. To see whether letting the Op*l* orbitals be active introduces significant changes, the present CAS(8,8) calculations were extended to CASCI(12,10) calculations by adding to the CAS(8,8) space the two p-type lone-pair orbitals (and their four electrons) from the split-localized orbitals found in the CAS(8,8) calculation.[62] These CASCI-(12,10) calculations yield energies that differ from the CAS(8,8) energies reported in Table 1 by the following amounts

Points on the MEP,	$E(8,8) - E(12,10)$ (kcal/mol)
diox	1.00
TS	0.78
RPP1	1.14
RPP2	1.46
SP	1.43
RPP3	0.52
RPP4	0.61
$2(H_2CO)$	0.62

The inclusion of the Op*l* orbitals in the active space makes no essential difference for the ground state because the Op*l* orbitals remain doubly occupied also in the CASCI(12,10) calculation. Thus, the CAS(8,8) approach accounts for the same relevant interactions as the CASCI(12,10) approach along the entire reaction paths.[63]

(ii) The calculations in the cited investigations[21,23] account for some dynamic correlation through the addition of second-order perturbation corrections to CASSCF calculations. The present study includes only non-dynamic correlation. Nevertheless, there is marked qualitative agreement on the overall shape of the MEP displayed in Figure 2. This agreement is exhibited by a comparison of the relevant energy differences, i.e.:

the dissociation energy

$$= [E(\text{dioxetane}) - 2E(\text{formaldehyde})]$$

the dissociation barrier $= [E(\text{TS}) - E(\text{dioxetane})]$

the shallow decay of the MEP in the biradical region

$$= [E(\text{TS}) - E(\text{SP})]$$

These energy differences are shown in Table 5 for the calculations of refs 21−23 and for the present work. The known experimental values are also listed.

(iii) Since the chemiluminescent light is emitted from a triplet state, intersystem crossing from the singlet ground state (S_o) to the lowest triplet state (T_1) occurs during dissociation. The cited calculations[21,23] have shown that, on the biradical part of the MEP, the singlet and the triplet states are close in energy[64−66] and that the ground-state PES stays relatively level in the vicinity of the MEP in some coordinate directions.

DOI: 10.1021/acs.jpca.5b03402
J. Phys. Chem. A 2015, 119, 10376−10389

These features are also reproduced by the present CAS(8,8) calculations on the biradical part of the MEP. The lowest MCSCF optimized triplet state T_1 differs in energy from the ground state S_o by the amounts

points on the MEP	TS	RPP1	RPP2	SP	RPP3
$E(T_1) - E(S_o)$ (kcal/mol)	3.20	0.03	0.03	0.03	0.55

Thus, the two states come very close in the CAS(8,8) space.

An estimate of the flatness of the valley around the ground-state MEP is obtained from the magnitudes of the frequencies ν_k of the projected nuclear Hessian in the space normal to the MEP gradient. Several of these ν_k were found to have values of $h\nu_k$ between 0.31 and 1.88 kcal/mol on the MEP between TS and SP. Since one frequency is imaginary everywhere between the valley−ridge inflection point VRI and the saddle point SP, ground state dynamic trajectories can be expected to be deflected from this ridge on the MEP toward the ground state products. Since the part between VRI and SP constitutes ∼40% of the range for which the states T_1 and S_o are really close, this deflection would compete with the intersystem crossing and favor the formaldehyde ground states, which make up more than half of the product distribution.[5] The agreements found in this section support the validity of the physical interpretations that were developed in the preceding sections.

6. CONCLUSIONS

The present investigation establishes that the quasi-atomic analysis formulated in the previous papers[1,2] is in fact able to successfully extract from rigorous MCSCF wave functions along a nontrivial reaction path an interpretation of bonding changes that fits into the qualitative chemical expectations, and it additionally provides quantitative energetic specifications.

The ground state dissociation of dioxetane into the formaldehyde dimer is analyzed along the MEP in terms of QUAOs. The QUAOs are found to evolve smoothly with little change in shape throughout the reaction. The changes of the covalent interactions along the reaction path are quantitatively identified by the changes in the orbital populations and, notably, in the KBOs, a new quantitative measure introduced in the present analysis.

The dissociation is found to be a two-stage bifurcating reaction. The MEP consists of two sections with starkly different properties, which reflect basic changes in the physical nature that the system undergoes along the dissociation path.

In the first stage, the oxygen−oxygen bond breaks, and the QUAOs that had formed the weak OO bond become singly occupied radical QUAOs on the oxygen atoms. Weak covalent interactions continue to exist between them at the transition state TS. The MEP, which starts in C_2 symmetry at dioxetane, continues in this symmetry through and beyond the transition state TS. On the subsequent gentle descent, the MEP passes through a valley−ridge inflection point to a second saddle point SP, which lies ∼3 kcal/mol below the transition state TS. On this section, the lowest triplet state comes within 0.025 kcal/mol of or possibly intersects the ground state singlet MEP. At the saddle point SP and perpendicular to the incoming C_2 MEP, two new MEPs of C_1 symmetry start in opposite directions, which plunge on very steep descents to two equivalent formaldehyde dimers of C_{2h} symmetry.

The breakage of the CC bond and the concomitant formation of the π-bonds in each formaldehyde fragment occur in close vicinity of the saddle point SP. The bonding rearrangements involve a change in the character of the p-lone-pair QUAOs on oxygen. At the beginning of the second MEP, shortly after the start of the descent from the saddle SP, the CC bond elongates and weakens sufficiently so that the QUAOs that form this bond become available for other interactions. Simultaneously, the increase in the dihedral OCC′O′ angle to ∼68° weakens the interactions of the radical QUAOs on oxygen. As a result, the radical QUAO on each oxygen becomes a doubly occupied lone pair, and the former p-lone-pair QUAO on oxygen becomes singly occupied and begins to form a π-bond with the carbon QUAO that previously had been engaged in the CC bond. The establishment of the CO π-bond leads to an electron population increase on each oxygen and a corresponding electron population decrease on each carbon.

According to these results, the breakage of the CC and OO bonds and the formation of the CO π-bonds do not occur in a concerted manner but in a two-stage process. The right-angle turn of the MEP at the saddle point SP and the concomitant discontinuity in the slope of the energy at this point result from the very different physical characteristics of the two parts of the MEP, namely, a gentle descent in C_2 symmetry from TS to SP, due to a strong CC bond and weak interactions of the oxygen radicals, versus a steep descent in C_1 symmetry from SP to the dimer, due to a weakened CC bond and strong CO π-bond formation.

The results of the present investigation complement previous studies of the dioxetane dissociation, which focused on elucidating the origin of the radiationless singlet−triplet transition that causes the chemiluminescence. There is agreement on the existence of a biradical structure on the reaction path and on the near degeneracy of the singlet and triplet states on this biradical part of the MEP. The insights provided by the QUAO analysis for the singlet state suggest that this approach should also be instructive for the triplet state.

AUTHOR INFORMATION

Corresponding Author

*Phone: 515-294-5253. E-mail: ruedenberg@iastate.edu.

Notes

The authors declare no competing financial interest.

ACKNOWLEDGMENTS

The authors thank Dr. Emilie Guidez for performing the EFP calculation on the formaldehyde dimer. They also thank Dr. Joseph Ivanic for stimulating discussions and information regarding dioxetane-like structures in large molecules. The present work was supported by the National Science Foundation under Grant No. CHE-1147446 to Iowa State Univ. In part, the work was also supported (for K.R.) by the U.S. Department of Energy, Office of Basic Energy Sciences, Division of Chemical Sciences, Geosciences & Biosciences through the Ames Laboratory at Iowa State Univ. under Contract No. DE-AC02-07CH11358.

REFERENCES

(1) West, A. C.; Schmidt, M. W.; Gordon, M. S.; Ruedenberg, K. A Comprehensive Analysis of Molecule-intrinsic Quasi-atomic, Bonding, and Correlating Orbitals. I. Hartree-Fock Wave Functions. *J. Chem. Phys.* **2013**, *139*, 234107 hereafter referred to as Paper I..

(2) West, A. C.; Schmidt, M. W.; Gordon, M. S.; Ruedenberg, K. A Comprehensive Analysis of Molecule-intrinsic, Quasi-atomic Orbitals. II. Strongly Correlated MCSCF Wave Functions. *J. Phys. Chem. A* **2015**; 150916123848008; hereafter referred to as Paper II. 10.1021/acs.jpca.5b03399

DOI: 10.1021/acs.jpca.5b03402
J. Phys. Chem. A 2015, 119, 10376−10389

(3) West, A. C.; Schmidt, M. W.; Gordon, M. S.; Ruedenberg, K. A Comprehensive Analysis in Terms of Molecule-intrinsic, Quasi-atomic Orbitals. III. The Covalent Bonding Structure of Urea. *J. Phys. Chem. A* **2015**, 150915114548004.
(4) Fukui, K. Formulation of the Reaction Coordinate. *J. Phys. Chem.* **1970**, *74*, 4161−4163.
(5) Adam, W. A.; Baader, W. J. Effects of Methylation on the Thermal Stability and Chemiluminescence Properties of 1,2-Dioxetanes. *J. Am. Chem. Soc.* **1985**, *107*, 410−416 This paper contains references to numerous other works on this problem.
(6) Hummelen, J. C.; Luider, T. M.; Oudman, D.; Koek, J. N.; Wynberg, H. In *Luminescence Techniques in Chemical and Biochemical Analysis;* Willy, R. G., Baeyens, D. D. K., Korkidis, K., Eds.; Marcel Dekker: New York, 1991, pp 567−598.
(7) Adam, W. The Chemistry of 1,2-Dioexetanes. *Adv. Heterocycl. Chem.* **1977**, *21*, 437−481 gives a general discussion of dioxetane chemistry.
(8) Clennan, E. L.; Nagraba, K. Additions of Singlet Oxygen to Alkoxy-substitued Dienes. The Mechanism of the Singlet Oxygem 1,2-cycloaddition Reaction. *J. Am. Chem. Soc.* **1988**, *110*, 4312−4318.
(9) Bartlett, P. D.; Mendenhall, G. D.; Schaap, A. P. Competitive Modes of Reaction of Singlet Oxygen. *Ann. N. Y. Acad. Sci.* **1970**, *171*, 79−88.
(10) Asveld, E. W. H.; Kellogg, R. M. Formation of 1,2-Dioxetanes and Probable Trapping of an Intermediate in the Reactions of some Enol Ethers with Singlet Oxygen. *J. Am. Chem. Soc.* **1980**, *102*, 3644−3646.
(11) Maranzana, A.; Ghigo, G.; Tonachini, G. Diradical and Peroxirane Pathways in the [π2+π2] Cycloaddition Reactions of $^1\Delta_g$ Dioxygen with Ethene, Methyl Vinyl Ether, and Butadiene: A Density Functional and Multireference Perturbation Theory Study. *J. Am. Chem. Soc.* **2000**, *122*, 1414−1423.
(12) Gorka, A. P.; Nani, R. R.; Zhu, J. J.; Mackem, S.; Schnermann, M. J. A Near-IR Uncaging Strategy Based on Cyanine Photochemistry. *J. Am. Chem. Soc.* **2014**, *136*, 14153−14159.
(13) Engel, E.; Schraml, R.; Maisch, T.; Kobuch, K.; König, B.; Szeimies, R. M.; Hillenkamp, J.; Bäumler, W.; Vasold, R. Light-induced Decomposition of Indocyanine Green. *Invest. Ophthalmol. Visual Sci.* **2008**, *49*, 1777−1783.
(14) Desiraju, G. R.; Steiner, T. *The weak hydrogen bond,* IUCr Monographs on Crystallography; Oxford University Press: 1999.
(15) Hobza, P.; Zahradnik, R.; Müller-Dethlefs, K. The World of Non-covalent Interactions. *Collect. Czech. Chem. Commun.* **2006**, *71*, 443−531.
(16) Schneider, H. J. Binding Mechanisms in Supramolecular Complexes. *Angew. Chem., Int. Ed.* **2009**, *48*, 3924−3977.
(17) Thakur, T. S.; Kirchner, M. T.; Bläser, D.; Boese, R.; Desiraju, G. R. Nature and Strength of CH···O Interactions involving Formyl Hydrogen Atoms: Computational and Experimental Studies of small Aldehydes. *Phys. Chem. Chem. Phys.* **2011**, *13*, 14076−14091.
(18) Vargas, R.; Garza, J.; Dixon, D. A.; Hay, B. P. How Strong is the C$^{\alpha}$H···O═C Hydrogen Bond? *J. Am. Chem. Soc.* **2000**, *122*, 4750−4755.
(19) Devarajan, A.; Markutsya, S.; Lamm, M. H.; Cheng, X.; Smith, J. C.; Baluyut, J. Y.; Kholod, Y.; Gordon, M. S.; Windus, T. L. Ab initio Study of Molecular Interactions in Cellulose Iα. *J. Phys. Chem. B* **2013**, *117*, 10430−10433.
(20) Johnston, R. C.; Cheong, P. H. C-H···O Non-classical Hydrogen Bonding in the Stereomechanics of Organic Transformations: Theory and Recognition. *Org. Biomol. Chem.* **2013**, *11*, 5057−5064.
(21) Reguero, M.; Bernardi, F.; Bottoni, A.; Olivucci, M.; Robb, M. A. Chemiluminescent Decomposition of 1,2-Dioxetanes: an MC-SCF/MP2 study with VB Analysis. *J. Am. Chem. Soc.* **1991**, *113*, 1566−1572.
(22) Wilsey, S.; Bernardi, F.; Olivucci, M.; Robb, M. A.; Murphy, S.; Adam, W. The Thermal Decoposition of 1,2-Dioxetane Revisited. *J. Phys. Chem. A* **1999**, *103*, 1669−1677.
(23) De Vico, L.; Liu, Y. J.; Krogh, J. W.; Lindh, R. Chemiluminescence of 1,2-Dioxetane. Reaction Mechnism Uncovered. *J. Phys. Chem. A* **2007**, *111*, 8013−8019.
(24) Farahani, P.; Roca-Sanjuan, D.; Zapata, F.; Lindh, R. Revisiting the Nonadiabatic Process in 1,2-Dioxetane. *J. Chem. Theory Comput.* **2013**, *9*, 5404−5411.
(25) Dolgonos, G. A. Which Isomeric Form of Formaldehyde Dimer is the most stable - a High-level Coupled-cluster Study. *Chem. Phys. Lett.* **2013**, *585*, 37−41 which also contains references to prior literature..
(26) Note however that the actual experimental synthesis of dioxetane reported in ref 5 was achieved by the preparation of 1-bromo-2-hydroperoxypropane and subsequent BrH abstraction from this intermediate.
(27) Tonachini, G.; Schlegel, H. B.; Bernardi, F.; Robb, M. A. MC-SCF Study of the Addition Reaction of the $^1\Delta_g$ Oxygen Molecule to Ethene. *J. Am. Chem. Soc.* **1990**, *112*, 483−491.
(28) Hua, H.; Ruscic, B.; Wang, B. Theoretical Calculations on the Reaction of Ethylene with Oxygen. *Chem. Phys.* **2005**, *311*, 335−341.
(29) Park, K.; West, A.; Raheja, E.; Sellner, B.; Lischka, H.; Windus, T. L.; Hase, W. L. Singlet and triplet Potential Surfaces for the O_2+C_2H_4 Reaction. *J. Chem. Phys.* **2010**, *133*, 184306.
(30) Sun, R.; Park, K.; de Jong, W. A.; Lischka, H.; Windus, T. L.; Hase, W. L. Direct Dynamics Simulation of Dioxetane Formation and Decomposition via the singlet ·O-O-CH_2-CH_2· Biradical: non-RRKM Dynamics. *J. Chem. Phys.* **2012**, *137*, 044305.
(31) See, for example, the discussion in Section 4.3 of ref 2.
(32) Schmidt, M. W.; Baldridge, K. K.; Boatz, J. A.; Elbert, S. T.; Gordon, M. S.; Jensen, J. H.; Koseki, S.; Matsunaga, N.; Nguyen, K. A.; Su, S.; Windus, T. L.; Dupuis, M.; Montgomery, J. A. General Atomic and Molecular Electronic Structure System. *J. Comput. Chem.* **1993**, *14*, 1347−1363.
(33) Gordon, M. S.; Schmidt, M. W. In *Theory and Applications of Computational Chemistry, the first forty years;* Dykstra, C. E., Frenking, G., Kim, K.S., Scuseria, G. E., Eds.; Elsevier: Amsterdam, 2005; pp 1167−1189.
(34) Dunning, T. H., Jr. Gaussian Basis Sets for use in Correlated Molecular Calculations. I. The atoms Boron through Neon and Hydrogen. *J. Chem. Phys.* **1989**, *90*, 1007−1023.
(35) Gonzalez, C.; Schlegel, H. B. An Improved Algorithm for Reaction Path Following. *J. Chem. Phys.* **1989**, *90*, 2154−2161.
(36) The ring strain was obtained by an MP2 calculation of the reaction energy for the isodesmic reaction [$O_2C_2H_4$(dioxetane) + $2CH_4$ + $2H_2O$ → HOOH + $2H_3COH$ + H_3CCH_3]. A reaction energy of 13.81 kcal/mol (left side minus right side) was obtained when the OO bond length and the CO bond length in dioxetane were shortened to be identical with those in the molecules on the right side of the isodesmic reaction equation. When the actual geometry of dioxetane was used, the reaction energy was 4.39 kcal/mol. Zero point vibrational energies were not included for the present purpose. Regarding the method, see Fuchs, R. The Evaluation of Strain and Stabilization in Molecules Using Isodesmic Reactions. *J. Chem. Educ.* **1984**, *61*, 133−135.
(37) According to a group theoretical analysis, the molecular symmetry group and the representation of the wave function do not change along any steepest descent path with a continuous non-vanishing gradient. Furthermore, the symmetry group on the steepest descent path must be a subgroup of the symmetry groups at the critical points at the start and at the end of the path. The representations of the relevant eigenmodes of the Hessians at these critical points are related to the representation of the wave function on the steepest descent path by subduction. The representation of the gradient is totally symmetric all along the steepest descent path. More complicated relationships hold at points where the steepest descent path crosses an intersection seam between PESs. See, for example, references 4 and 38−41.
(38) Murrell, J. N.; Laidler, K. J. Symmetries of Activated Complexes. *Trans. Faraday Soc.* **1968**, *64*, 371−377.
(39) Murrell, J. N.; Pratt, G. L. Statistical Factors and the Symmetry of Transition States. *Trans. Faraday Soc.* **1970**, *66*, 1680−1684.

DOI: 10.1021/acs.jpca.5b03402
J. Phys. Chem. A 2015, 119, 10376−10389

(40) McIver, J. W.; Komornicki, A. Rapid Geometry Optimization for Semi-empirical Molecular Orbital Methods. *Chem. Phys. Lett.* **1971**, *10*, 303−306.
(41) McIver, J. W. Structures of Transition States. Are they Symmetric? *Acc. Chem. Res.* **1974**, *7*, 72−77.
(42) Valley Ridge Inflection points on steepest descent paths were introduced by P. Valtazanos and K. Ruedenberg [see ref 43], who quantitatively analyzed the associated PES and steepest descent patterns in relation to the transition states. The analysis elucidated a bifurcation on the global PES for the ring opening of cyclopropylidene [see refs 44 and 45]. The existence of such points had previously been noted by ref 46.
(43) Valtazanos, P.; Ruedenberg, K. Bifurcations and Transition States. *Theor. Chim. Acta.* **1986**, *69*, 281−307.
(44) Valtazanos, P.; Elbert, S. T.; Xantheas, S.; Ruedenberg, K. The ring opening of cyclopropylidene to allene: global features of the reaction surface. *Theor. Chim. Acta.* **1991**, *78*, 287−326.
(45) Xantheas, S.; Elbert, S. T.; Ruedenberg, K. The ring opening of cyclopropylidene to allene: key features of the accurate reaction surface. *Theor. Chim. Acta.* **1991**, *78*, 365−395.
(46) Metiu, H.; Ross, J.; Silbey, R.; George, T. F. On symmetry properties of reaction coordinates. *J. Chem. Phys.* **1974**, *61*, 3200−3209.
(47) Ess, D. H.; Wheeler, S. E.; Iafe, R. G.; Xu, L.; Celebi-Ölcüm, N.; Houk, K. N. Bifurcations on Potential Energy Surfaces of Organic Reactions. *Angew. Chem., Int. Ed.* **2008**, *47*, 7592−7601.
(48) Harabuchi, Y.; Taketsugu, T. A Significant Role of the Totally Symmetric Valley-Ridge Inflection Point in the Bifurcating Reaction Pathway. *Theor. Chem. Acc.* **2011**, *130*, 305−315.
(49) Rehbein, J.; Carpenter, B. K. Do we fully Understand what Controls Chemical Selectivity? *Phys. Chem. Chem. Phys.* **2011**, *13*, 20906−20922.
(50) Takagi, K.; Oka, T. Millimeter Wave Spectrum of Formaldehyde. *J. Phys. Soc. Jpn.* **1963**, *18*, 1174−1180.
(51) This identification is a basic achievement of the present approach. It is described in ref 1 (Section V.A.1) for HF wave functions and in ref 2 (Section 4.3) for MCSCF wave functions.
(52) Specifically, the transition from a bonding/antibonding orbital pair to two radical orbitals is a result of the criterion that separates strongly and weakly occupied natural orbitals, as described in the fourth paragraph of Section 4.1 in reference 2.
(53) The present analysis uses the quasi-atomic orbitals that were denoted as "unrestrained" in Sections 4.2.2 and 4.3 of ref 2, which are the standard choice of the present method. The "restrained" QUAOS are for special situations as discussed in the mentioned Sections of ref 2.
(54) Schmidt, M. W.; Ivanic, J.; Ruedenberg, K. Covalent Bonds are Created by the Drive of Electron Waves to Lower their Kinetic Energy through Expansion. *J. Chem. Phys.* **2014**, *140*, 204104.
(55) Schmidt, M. W.; Ivanic, J.; Ruedenberg, K. The Physical Origin of Covalent Bonding. In *The Chemical Bond, Fundamental Aspects of Chemical Bonding;* Frenking, G., Shaik, S., Eds.; Wiley-VCH: Weinheim, Germany, 2014; pp 1−67.
(56) Coulson, C. A.; Longuet-Higgins, H. C. The Electronic Structure of Conjugated Systems. I. General Theory. *Proc. R. Soc. London, Ser. A* **1947**, *191*, 39−60.
(57) Chirgwin, B. H. Summation Convention and the Density Matrix in Quantum Theory. *Phys. Rev.* **1957**, *107*, 1013−1025.
(58) See Section 3.3 of ref 2.
(59) Gordon, M. S.; Freitag, M. A.; Bandyopadhyay, P.; Jensen, J. H.; Kairys, V.; Stevens, W. J. The Effective Fragment Potential Method: a QM-based MM Approach to Modeling Environmental Effects in Chemistry. *J. Phys. Chem. A* **2001**, *105*, 293−307.
(60) Gordon, M. S.; Slipchenko, L. V.; Li, H.; Jensen, J. H. The Effective Fragment Potential: a General Method for Predicting Intermolecular Interactions. *Annu. Rep. Comput. Chem.* **2007**, *3*, 177−193.
(61) Gu, Y.; Kar, T.; Scheiner, S. Fundamental Properties of the CH···O Interaction: is it a true Hydrogen Bond. *J. Am. Chem. Soc.* **1999**, *121*, 9411−9422.
(62) The explicit generation of this (12,10) CI space was as follows. In the upper part of Figure 3, four of the split-localized orbitals are seen to be lone-pair orbitals on the two oxygen atoms (note that the right side of the molecule is not pictured). For *all* points from TS to SP, the split-localization method in fact results in a strict separation of 2s-type lone pair orbitals and 2p-type lone pair orbitals. In the case of the CAS(8,8) calculations, all four lone-pair split-localized orbitals lie in the inactive space labeled (i) in Section 2. The CAS(12,10) space was then generated by moving the two 2p-type split-localized orbitals and their four electrons from the inactive space (i) to the active space (ii).
(63) The inclusion of the Op$'$ orbitals in the active space is of course required for the description of the dissociation of the T_1 triplet state to the separated formaldehyde monomers with one of them being in the $^3(n\rightarrow p^*)$ excited state.
(64) That the intersystem crossing is a result of intermediate biradical structures with a (near-)degeneracy between triplet and singlet was first suggested by refs 65 and 66. Other mechanisms were however also postulated. A discussion of early work is given in refs 21 and 22.
(65) O'Neal, H. E.; Richardson, W. H. Thermochemistry of 1,2-dioxetane and its methylated derivatives. Estimate of activation parameters. *J. Am. Chem. Soc.* **1970**, *92*, 6553−7.
(66) Harding, L. B.; Goddard, W. A. Intermediates in the chemiluminescent reaction of singlet oxygen with ethylene. Ab initio studies. *J. Am. Chem. Soc.* **1977**, *99*, 4520−3.

DOI: 10.1021/acs.jpca.5b03402
J. Phys. Chem. A 2015, 119, 10376−10389